RESEARCH ARTICLE

Macromolecular Chemistry and Physics
www.mcp-journal.de

The Semicrystalline Morphology of Polybutylene Succinate Supports a General Scheme Based on Intracrystalline Dynamics

Qiang Yu, Afiq Anuar, Albrecht Petzold, Jens Balko, Kay Saalwächter, and Thomas Thurn-Albrecht**

Based on a limited set of model samples it has been recently shown that semicrystalline polymers exhibit different morphological characteristics depending on the existence and timescale of intracrystalline chain diffusion (ICD) relative to the kinetics of crystal growth. Here, the generality of these reports for the case of so-called crystal-fixed polymers without or very slow ICD is tested by providing a detailed nuclear magnetic resonance (NMR) and small-angle X-ray scattering analysis of polybutylene succinate (PBS), a biodegradable polyester. By using a combination of NMR techniques covering different timescales it is shown that there is no intracrystalline dynamics on a time scale faster than 1 s, that is, PBS is crystal-fixed. An expected crystallinity below 50% and the typical morphology consisting of lamellar crystals with a well-defined crystal thickness and a broad thickness distribution of the amorphous interlayers are confirmed. By combining these results with differential scanning calorimetry measurements, a more precise value could be provided for the enthalpy of melting than previously available. The mechanical properties at room temperature are furthermore influenced by additional insertion crystallization taking place during cooling, which leads to an increase of the mechanical modulus by a factor of ≈2.5 as compared to the state at the end of isothermal crystallization.

1. Introduction

The nanoscopic morphology of semicrystalline polymers consisting of stacks of thin lamellar crystals separated by amorphous interlayers determines to a large extent their mechanical properties,[1] which are generally important for application requirements and which are also an important criterion that nowadays hinders the replacement of commodity polymers by biodegradable or biobased polymers. Given its relevance, the question has been under investigation for a long time, but there is until today no general consensus about the factors that determine the morphology, that is, the thickness of both the crystalline and of the amorphous layers. Several theoretical models have been proposed. The classical kinetic models assume that crystals with the highest growth rate dominate the crystal morphology. It was assumed that growth is limited by an activated process,[2,3] such as secondary nucleation, removal of pinning defects[4,5] or by chain dynamics.[6] In multistage models it is assumed that crystal thickness is a result of reorganization processes taking place during or after crystallization. Different processes have been suggested to be responsible for reorganization, namely intracrystalline chain dynamics (ICD) related to an α_c-relaxation,[7–9] size-dependent stability of different crystal phases[10] or a mesophase with lower order.[11,12] All these models do not distinguish between crystal-mobile polymers that have an α_c-relaxation and crystal-fixed polymers that display no α_c-relaxation.

We recently proposed that this distinction is essential for the formation of the semicrystalline morphology,[13] and showed that the competition between crystal growth and crystal reorganization determines the semicrystalline morphology. Thanks to the quantitative access to the ICD via dedicated solid-state nuclear magnetic resonance (NMR) techniques we were able to quantify this relation and showed that the ratio τ_{lc}/τ_c is the decisive parameter.[14] Here τ_{lc} is the layer crystallization time, the time during which the crystal grows on average by one molecular layer, and $\langle\tau_c\rangle$ is the so-called jump correlation time determined by NMR, the average time between two helical defect jumps, which corresponds to the α_c-relaxation time. Starting

Q. Yu, A. Anuar, A. Petzold, K. Saalwächter, T. Thurn-Albrecht
Institute of Physics
Martin Luther University Halle-Wittenberg
06099 Halle, Germany
E-mail: kay.saalwaechter@physik.uni-halle.de;
thurn-albrecht@physik.uni-halle.de
J. Balko
Processing Center for Biopolymers
Fraunhofer Institute of Applied Polymer Research (IAP)
01987 Schwarzheide, Germany

The ORCID identification number(s) for the author(s) of this article can be found under https://doi.org/10.1002/macp.202200459

DOI: 10.1002/macp.202200459

from polymers with slow ICD ($\tau_{lc} \ll \tau_c$), over medium ICD ($\tau_{lc} \approx \tau_c$) to fast ICD ($\tau_{lc} \gg \tau_c$), the crystal thickness increases. The different regimes also result in different features in the semicrystalline morphology.[13] Crystal-fixed polymers such as PCL (polycaprolactone) with slow ICD form crystals with a rather uniform crystal thickness, close to the thermodynamic stability limit and a broader distribution for the amorphous-layer thickness. Crystal-mobile polymers on the other hand such as PEO (polyethyleneoxide) with fast ICD show a well-defined thickness of the amorphous regions but broadly distributed crystal thicknesses. These features can be worked out by quantitative modeling of small-angle X-ray scattering (SAXS) data.[13,15] In addition, the competition also influences the thermal properties of the crystals.[16] During heating the crystals of crystal-mobile polymer thicken to gain stability. The crystals of crystal-fixed polymer, on the other hand, melt and recrystallize during heating to form more stable crystals.

Based on these insights, we here want to crosscheck this scheme on another relevant polymer, namely polybutylenesuccinate (PBS), a biodegradable polyester. PBS is one of the most successful candidates for replacing the commodity plastic polyethylene (PE) because it has similar thermal properties and its mechanical properties are not substantially inferior to those of PE.[17,18] PE, the most consumed polymer because of its superb thermal and mechanical properties,[17,19] is crystal-mobile polymer,[20,21] but it is not well recyclable nor biodegradable.[22] Compared with PE, PBS is still not widely studied and there is no quantitative assessment of intracrystalline dynamics and the semicrystalline morphology. Xu et al.[23] and Schick et al.[24] studied the crystal thickness by SAXS and Differential scanning calorimetry (DSC), respectively. The crystallinity was estimated based on wide angle X-ray scattering (WAXS) by Papageorgiou,[25] but this method has in most cases limited accuracy. Di Lorenzo et al.[26] and Schick et al.[27] showed that crystallinity of PBS is temperature dependent, but the crystallinity at room temperature, which is critical for applications, is not available. Available values for the enthalpy of melting ($\Delta H_{m,100}$) determined by different methods range from 110, over 200 to 210 J mol^{-1}.[25,28,29]

We therefore here present an experimental study to probe the potential ICD of PBS by a combination of solid-state NMR techniques in combination with a SAXS-based analysis of the complete semicrystalline morphology. The combination of these different robust methods was used to determine the crystallinity and its dependence on temperature. In addition, we provide a more reliable value for $\Delta H_{m,100}$.

2. Result and Discussion

2.1. Is PBS a Crystal-Fixed Polymer?

To determine if PBS is a crystal-fixed polymer, we need to compare the timescale of possible intracrystalline chain diffusion (ICD) with the layer crystallization time τ_{lc}.[13] To study fast molecular dynamics on the time scale of µs in the crystalline fraction of PBS, we performed ^{1}H-NMR free induction decay (FID) measurements. In addition, these measurements allows us to determine the crystallinity, which we separately discuss further below. After isothermal crystallization at 100 °C, the sample was cooled to 30 °C and heated step-wise to 115 °C. At each temperature, an FID measurement was taken and the normalized crystal fraction was extracted according to Equation (4) in Experimental Section. The resulting FIDs for the crystalline fractions are shown in **Figure 1**. All curves show the typical shape for an organic solid with strong ^{1}H dipole-dipole couplings, here without any significant changes with temperature.[30] The temperature independence of the curves indicates the absence of ICD on the time scale of the method (≈0.2 ms). If there was relevant ICD, we would observe temperature-dependent changes in the shape of the curves reflecting the increasingly fast molecular dynamics, where $\tau_c(T)$ typically follows an Arrhenius dependence.[13]

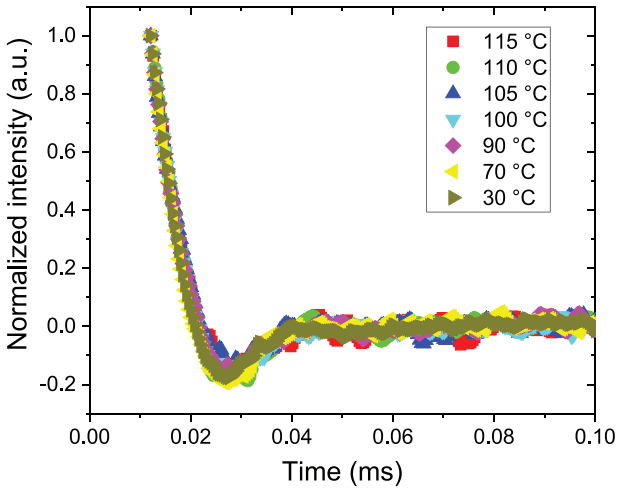

Figure 1. Normalized NMR-FID curves of the crystalline fraction of PBS crystallized at $T_c = 100$ °C measured at different temperatures as indicated in the legend. The fluctuations at larger times reflect the noise level. Note that data below 0.012 ms are missing due to the instrument dead time.

As no fast ICD was detected in PBS, we now need to address potentially slower motions up to the scale of seconds. Exchange-NMR methods relying on the reorientation of the ^{13}C chemical-shift anisotropy (CSA) tensor, as used in our previous work focusing on poly(oxymethylene),[14] are not applicable in the given case of PBS. The reason is the regularity of the crystal structure, specifically the all-trans rather than helical conformation, where the translation by one monomer unit places all atoms in crystallographically equivalent positions.[31] We are thus left with the possible detection of monomer exchange between the crystalline and amorphous regions, that is, probing the diffusive long-range ICD. This can be achieved either by observing an exchange between ^{13}C isotropic chemical shifts related to the two regions, provided they are distinguishable,[32] or by ^{13}C T_1 relaxation.[32,33]

The T_1-based approach relies on the usually very long T_1 of the crystalline ^{13}C, which show a T_1 decay rather by diffusing into the amorphous region where T_1 is often orders of magnitude shorter. The experiment is best realized by using Torchia's z-filtering pulse sequence[34] for the measurement of ^{13}C T_1 harnessing cross-polarization (CP) for signal enhancement, by which a decay curve with known final value of zero intensity is measured. In this way, deviations from single-exponential decay toward diffusive behavior are readily apparent.[33]

Prior to this, it is critical to determine which ^{13}C peak best represents the crystalline domain we are interested in, that is,

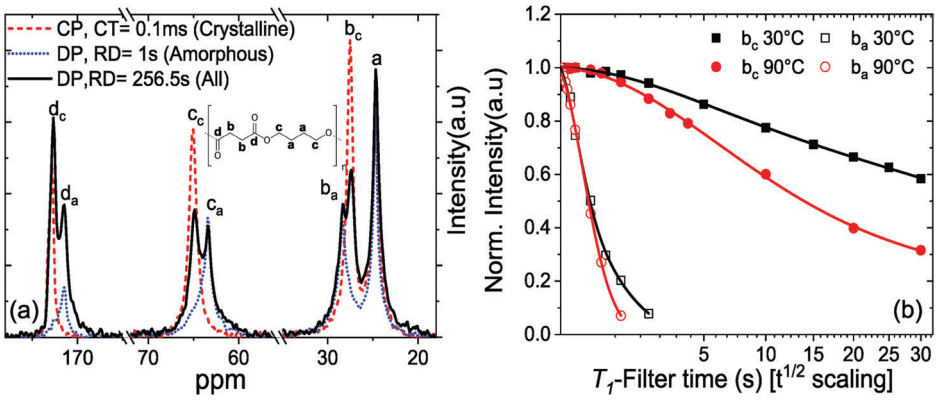

Figure 2. a) Comparison of ^{13}C spectra: ^{13}C CP MAS spectrum with 0.1 ms contact time (red), ^{13}C DP MAS spectra with RDs of 1 s (blue) and 265.5 s (black). The amorphous and crystalline contributions of each ^{13}C site (subscripts a and c, resp.) are thus easily assigned. b) T_1 relaxation decay versus the square-root of the waiting time of peak b_c after CP with 1.5 ms contact time at 30 and 90 °C. The solid lines are biexponential fits (see Table S1, Supporting Information for detailed results), where a shorter component with T_1 5–10 s can be assigned to the monomers closer to the interface.[36] The amorphous-phase decays for resonance b_a are also included for comparison. The *x*-axis scaling corresponds to $\sqrt{t}$, which would give a linear decay if the process were diffusive.

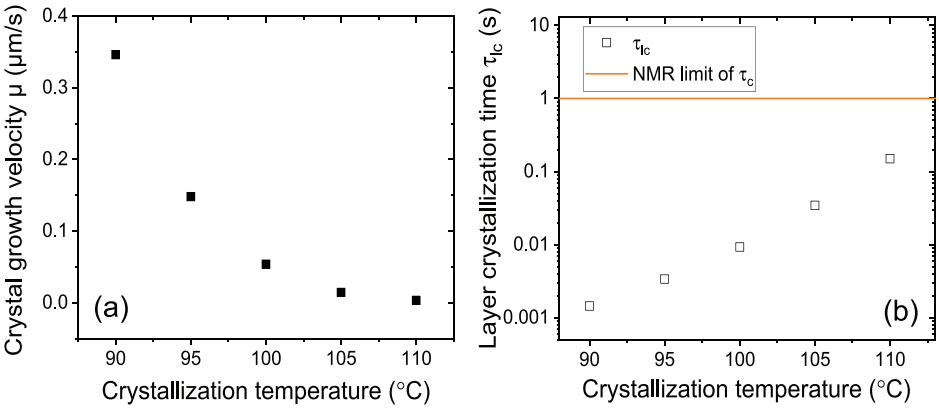

Figure 3. a) Crystal growth velocity μ of PBS vs. crystallization temperature. b) Corresponding layer crystallization time (τ_{lc}) and lower bound for the jump correlation time (τ_c) as a function of temperature.

avoiding signal contributions from the amorphous phase. To this end, we acquired ^{13}C spectra with 10 kHz magic-angle spinning (MAS), comparing CP and direct polarization (DP), see **Figure 2**a. As discussed in Experimental Section, the DP spectra with comparably short recycle delay (RD) show mostly amorphous signals and largely exclude the crystalline ones with their long T_1, while the latter are rather emphasized in CP spectra with short contact time (CT). A quantitative spectrum showing all resonances is obtained via a DP spectrum with an RD allowing for near-complete T_1 relaxation (≈250 s in our case). From their comparison, we can identify the crystalline (subscript c) and amorphous (a) resonances.

Based on the observed ^{13}C spectrum, the well-separated intense peak b_c was chosen to probe its T_1 relaxation and thus assess potential ICD. The T_1 decay curves of b_c for two rather different temperatures of 30 and 90 °C are shown in Figure 2b. These were obtained by using spectral deconvolution to avoid contribution from the neighboring peaks, see Figure S1, Supporting Information. The T_1 relaxation curves of peak b_c show no indication of a contribution of a more rapid decay ($T_1 < 1$ s) at both temperatures, and the initial decay is not linearized by the $\sqrt{t}$ scaling, as opposed to what would be observed if the decay were governed by diffusion of the monomers into the amorphous phase.[33] This implies the absence of ICD in PBS up to the timescale of about 1 s. PBS is this similar to the previously studied PCL, which was shown to be a crystal-fixed polyester,[35] see also Figure S1c, Supporting Information.

The layer crystallization time τ_{lc} can be estimated from the spherulitic growth velocity μ according to Equation (1)[13]

$$\tau_{lc} = \frac{5\forall}{\mu} \quad (1)$$

We measured μ of PBS during isothermal crystallization for different crystallization temperatures T_c. μ decreased with increasing T_c, accordingly τ_{lc} increased, as shown in **Figure 3**. The orange straight line in Figure 3b corresponds to the measurement threshold of τ_c estimated by NMR; τ_{lc} is lying well below this line for all T_c. Based on our previous results on PEO and PCL we would therefore expect that the semicrystalline morphol-

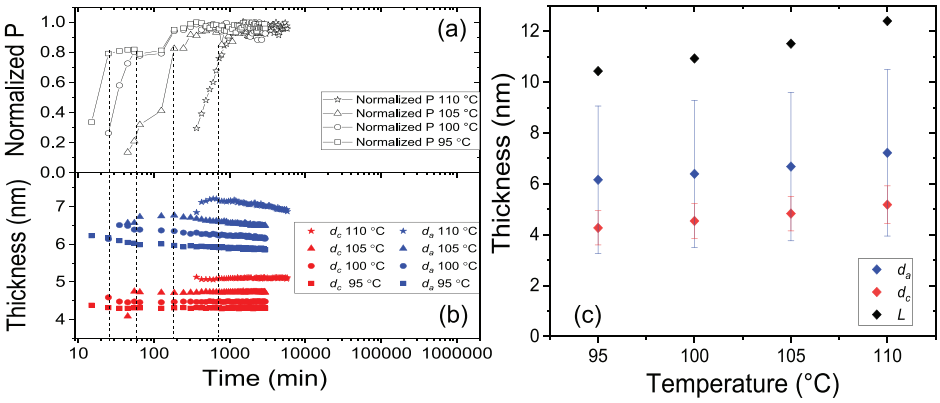

Figure 4. a) Porod parameter P and b) thickness of crystalline d_c and amorphous d_a layers during the course of isothermal crystallization at different temperatures (T_c = 95, 100, 105, and 110 °C). c) d_c, d_a and long period L versus crystallization temperature T_c, data obtained from the end point of each isothermal process in (b). Error bars indicate the distribution widths σ_c and σ_a.

ogy of PBS shows the typical features of a crystal-fixed polymer, that is, a well defined crystal thickness and a broad distribution for the thickness of the amorphous regions.[14]

2.2. Semicrystalline Morphology of PBS

To characterize the semicrystalline morphology of PBS we performed in situ SAXS measurements during isothermal crystallization over a broad range of crystallization temperatures. Using a 1D stack model for analysis (cf., Experimental Section), we determined the mean thickness of the crystalline and amorphous layers, d_c and d_a and their distribution widths, σ_c and σ_a. The results are shown in **Figure 4**. The Porod constant P is proportional to the specific crystalline-amorphous interface can therefore be used to follow the increase of crystallinity during the measurement. The time at which 80% of the final value was reached is marked by dashed vertical lines to indicate the transition from primary to secondary crystallization. As usual, the primary crystallization slows down strongly with increasing T_c. While d_c remains essentially unchanged during the whole course of crystallization, there is a reduction of d_a most likely caused by the growth of additional crystals in larger amorphous regions. Note that the distribution width for the crystal thickness σ_a is larger than the corresponding value for the amorphous regions, σ_c. Based on the results in Figure 4c, we obtained the volume crystallinity according to Equation (2).

$$X_{c,volume} = \frac{d_c}{d_c + d_a} \cdot 100\% \quad (2)$$

The mass crystallinity can be determined by taking the density of the crystalline and amorphous regions into account.

$$X_{c,mass} = \frac{\rho_c \cdot d_c}{\rho_c \cdot d_c + \rho_a \cdot d_a} \cdot 100\% \quad (3)$$

Here $\rho_c = 1.34\ g\ cm^{-3}$ is the density of the crystalline regions and $\rho_a = 1.18\ g\ cm^{-3}$ is the density of amorphous regions.[29] Both crystallinities are listed in **Table 1** together with the crystallinity measured by ^{1}H NMR FID, which was calculated according to Equation (5) in Experimental Section.

Table 1. Volume crystallinity $X_{c,\ volume}$ and mass crystallinity $X_{c,\ mass}$ as measured by SAXS and NMR, melting enthalpy ΔH_m from DSC (cf. below), and the average melting enthalpy of 100% crystalline PBS, $\Delta H_{m,100} = \Delta H_m / X_{mass}$ calculated from all shown values.

T_c [°C]	SAXS $X_{c,\ volume}$ [%]	SAXS $X_{c,\ mass}$ [%]	NMR $X_{c,\ mass}$ [%]	ΔH_m by DSC [J g^{-1}]	$\Delta H_{m,\ 100}$ [J g^{-1}]
95	42	45	41	77	
100	42	45	42	79	183±8
105	41	44	42	80	

The agreement between the crystallinities determined by SAXS and NMR is reasonable and within expectations, given the fact that the two methods rely on different principles. While SAXS relies on density contrast, the NMR-based FID deconvolution is based on mobility contrast. Additionally, the NMR analysis relies on a three-phase model, where Table 1 shows the value for the crystalline phase only. Based on the combined values an estimate for the enthalpy of melting can be given, as discussed below together with the DSC measurements. Our values for d_c are consistent with available literature values. These are SAXS based values from Xu et al. and an indirect estimate based on sophisticated DSC measurements and selected literature values for the enthalpy of melting, the equilibrium melting temperature and the free energy of the fold surface of lamellar crystals.[23,24] All of our results are consistent with our previous conclusions about the general morphological features of crystal-fixed polymers: A well-defined, relatively small crystal thickness d_c, absence of any observable crystal thickening, crystallinity X_c below 50%, greater values for σ_a than σ_c, while d_a and d_c show values of the same order of magnitude.[13,14]

2.3. Melting Behavior and Enthalpy of Melting

With the help of the known values of the crystallinity determined above, measurements of the enthalpy of melting of semicrystalline samples can be used to determine the extrapolated enthalpy of melting of a hypothetical 100% crystalline sample. **Figure 5** shows heating scans of PBS after isothermal crystalliza-

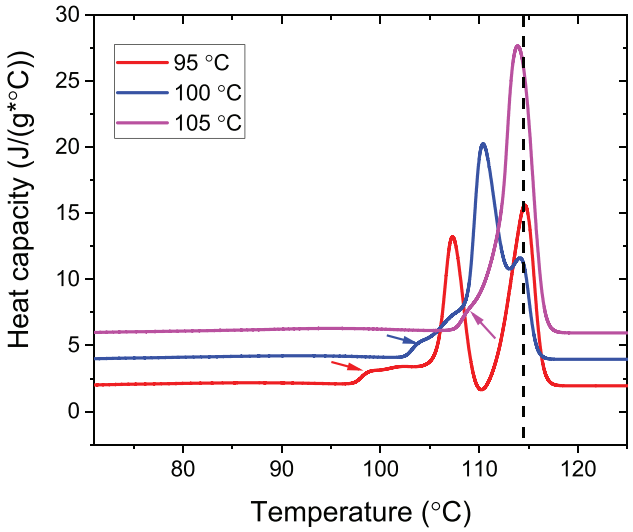

Figure 5. Heating scans of PBS at 10 K min^{-1} after isothermal crystallization at different temperatures T_c as indicated in the legend. The onset of melting is pointed out by arrows. The dashed line illustrates the approximately constant value of the final melting peak. The measurement for T_c = 100 °C and 105°C are shifted.

tion at different temperatures T_c. As observed before,[25,37,38] PBS shows multiple melting caused by melting and recrystallization, as it is typical for crystal-fixed polymers within a suitable parameter range.[16] The onset of melting, indicated by arrows is related to the stability of the crystals directly after crystallization. Accordingly, this feature shifted to higher temperatures with increasing crystallization temperature, while the final melting peak as a result of reorganization during heating by (repeated) melting and recrystallization appeared more or less at a the same temperature, independent of T_c.

To determine the melting enthalpies ΔH, we extrapolated the heat capacity from the molten state above 120 °C to T_c as base line and then integrated the heat capacity from T_c to 120 °C for each T_c. Division by the mass crystallinity gives an estimate for $\Delta H_{m,\,100}$. Note that this value $\Delta H_{m,\,100}$, is the enthalpy of melting at the temperature of melting, that is, ≈115 °C, not at the equilibrium melting temperature. The mean value is $\Delta H_{m,\,100}$ = 183 J g^{-1}, with a standard deviation of 8 J g^{-1}. This value is comparable but lower than those reported by other researchers of 200[29] and 210 J g^{-1}.[25] The latter value was determined in a similar way as above from the combination of a determination of the enthalpy of melting by DSC and of the crystallinity, in this case by WAXS. Given the limited precision of crystallinity values determined by WAXS, we believe that our value is more reliable. A third value of 110.3 J g^{-1} is often cited in the literature with reference to Chapter 5 of ref. [39] without giving a detailed derivation. $\Delta H_{m,\,100}$ itself is not given in there. Given the experimental results, this value can obviously be discarded.

2.4. Temperature-Dependent Crystallinity and Mechanical Modulus

A major motivation to characterize and understand the morphology of semicrystalline polymers is due to the fact that the mechanical properties, and specifically the modulus depend strongly on the crystallinity.[40,41] Based on specific DSC experiments, PBS is reported to crystallize further upon cooling below T_c, even if the previous isothermal crystallization at elevated temperatures was complete.[27,42] It is therefore of interest for practical application, for example, in packaging[43] to determine the crystallinity and the mechanical modulus in the temperature range between T_c and room temperature. While in DSC the changes in crystallinity are difficult to identify and separate from the heat capacity signal (cf., Figure S2, Supporting Information), they show up clearly in the NMR-FIDs.

The resulting temperature dependent crystallinity is shown in **Figure 6**a. After an isothermal crystallization at T_c = 100°C the sample was cooled to 30 °C and subsequently heated stepwise back to 100 °C with NMR measurements at each holding temperature. In this temperature range, the crystallinity changes more or less reversibly by a factor of ≈1.4. To confirm that the immobile phase formed during cooling is indeed crystalline, we performed WAXS measurements at selected temperatures, which show in fact an increase of the intensity of Bragg reflections at low temperatures, cf., Figure S3a, Supporting Information. Given the specific semicrystalline morphology, that is, $d_a > d_c$ and large σ_a, one would expect that this additional crystallization follows the scenario of insertion crystallization, that is, the thin crystals formed upon cooling grow into the larger amorphous regions. This picture is qualitatively consistent with observed changes in the SAXS data, shown in Figure S3b, Supporting Information. A similar effect was observed before for PCL, but weaker because of the smaller temperature difference between T_{room} and T_c.[13]

To investigate the effect of the observed changes in crystallinity on the linear mechanical properties we measured the dynamic shear modulus over the same temperature range at a fixed frequency. Samples with a similar thermal history as above (isothermal crystallization, T_c = 100 °C) were heated stepwise from 30 to 100 °C during the measurement, and then cooled again to 30 °C to confirm the reversibility of the measured values. The resulting values for G' and G'' are shown in Figure 6b. The storage modulus increases by a factor of about 2.5 during cooling over the relevant temperature range and the change in G'' is similar, while the absolute value is more than two orders of magnitude smaller. This behavior confirms that the temperature dependent changes are not caused by any relaxation. The results show that the additional crystallization upon cooling leads to a significant reinforcement of the material, which on the other hand also leads to a softening at elevated temperatures, effects which might be relevant for specific applications. We would expect that these are general effects for crystal-fixed polymers.

3. Conclusion

In conclusion, we could show that PBS has to be classified as a crystal-fixed polymer without or at most very slow intracrystalline chain diffusion, for which reorganization of the semicrystalline morphology plays no role during crystallization. In agreement with our hypothesis, PBS shows the typical morphological features that we previously attributed to this class of polymers, namely: a relatively small crystal thickness d_c with a weak dependence on crystallization temperature, absence of any discernible crystal thickening during isothermal crystallization; low

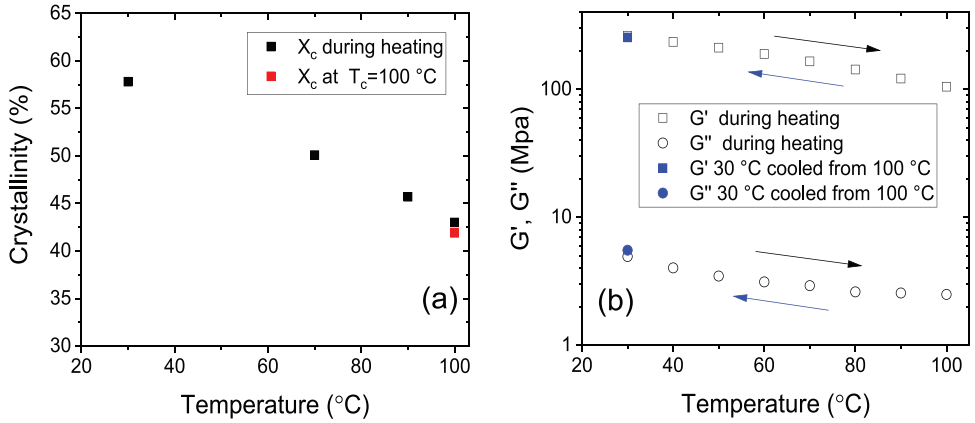

Figure 6. a) Crystallinity ($X_{c,\,mass}$) of PBS (T_c = 100 °C) measured by NMR-FID at different temperatures below T_c. The measurement at the end of the isothermal crystallization is represented by the red square. The sample was then cooled to 30 °C and the data shown as black symbols were acquired during heating. b) G′ and G″ versus temperature (10 rad s^{-1}, 0.1% strain). The externally crystallized sample (T_c = 100 °C) was also measured during heating (black squares). A final measurement was taken after subsequent cooling at 30 °C (blue symbols).

crystallinity (X_c < 50%), greater values for the distribution width σ_a of the amorphous regions than that for the crystalline layers σ_c. Similar to PCL, our previously studied model polymer, melting of the original crystals happens only slightly above T_c and during further heating a complicated melting and recrystallization process occurs leading to a final melting temperature largely independent of the crystallization temperature.

Making use of the large temperature range between crystallization/melting and room temperature, we could furthermore show that the crystallinity increases significantly during cooling by insertion crystallization, leading to rather strong increase in mechanical modulus.[13,14,16] Presumably, these are general effect for crystal-fixed polymers.

Based on the relatively precise and consistent values obtained for the crystallinity by two different experimental methods, we could extrapolate the measured value for the enthalpy of melting to the value of a 100% crystalline sample, $\Delta H_{m,\,100}$=183 ±8 J g^{-1}. Given the larger range of values for this quantity given previously in the literature, we believe that our value allows a more precise determination of the crystallinity based on simple DSC measurements.

With the decisive role of the intracrystalline chain diffusion for the morphology of semicrystalline polymers becoming more and more established, naturally the question arises which factors favor the existence and the time scale of such a dynamics. Polyesters promise to be interesting objects of study here, given the fact that, for example, PLA is known to exhibit ICD on an intermediate time scale.[44,45] A deeper understanding of the semicrystalline morphology of this polymer family would also be of practical interest as polyesters are promising candidates as commodity plastics because of their biodegradability and the fact that at least some of them are biobased.

4. Experimental Section

Materials:: A commercial-grade polybutylene succinate (FZ91) from PTT MCC Biochem Co., Ltd. with molecular weight M_n = 40 850 g mol^{-1}, M_w = 143 400 g mol^{-1} (*PD* = 3.5) was used as measured by GPC in dichloromethane with polystyrene calibration.

Proton Low-Resolution NMR FID Analyses:: ^{1}H time-domain NMR experiments at low field ($B_0 \approx 0.5$T) were performed on a Bruker minispec mq20 spectrometer with a proton frequency of about 20 MHz ($B_0 \approx 0.47$ T) using a static probe head with wide temperature range realized by heated or cooled air flow. The temperature accuracy of the instrument is ±1 K with a gradient of up to 0.5 K over the sample. The samples were always heated to 140 °C for 10 min to remove the thermal history, and then cooled to different crystallization temperatures for isothermal crystallization. The stepwise heating for the measurement shown in Figure 6a was carried out with a rate of ≈5 K min^{-1}, with an additional 10 min of equilibrium time before each NMR-FID measurement.

The instrument features a 90° pulse length of ≈2.8 µs; the recycle delay (RD), that is, the time between successive scans was set to 2 to 3 s, sufficient for near-complete T_1 relaxation. Measurements and analyses were conducted as reported in previous works.[30,46] To overcome problems with the dead time of about 12 µs, FID signals detected directly after a 90° pulse were compared with signals after a magic-sandwich echo (MSE). The latter avoided the dead time, but features some loss of intensity, meaning that shape parameters were taken from the MSE-FIDs while component amplitudes were taken from the FIDs.

The component decomposition was based upon the interplay of fast segmental dynamics in the amorphous phase and the strong ^{1}H–^{1}H dipole–dipole couplings, which meant that the very quick dipolar dephasing (short T_2) of the crystalline part was prolonged significantly for the amorphous protons. Typically, the FID of semicrystalline polymers above T_g can be decomposed into three components: a fast decay (crystalline fraction), a slow decay (amorphous fraction), and an intermediate decay (intermediate fraction), which was typically assigned to the interphase between crystalline and amorphous layers and was commonly assumed to be associated with the rigid amorphous fraction (often observed by DSC).

$$I_{FID}(t) = f_c \cdot e^{-(a^2t^2/2)} \cdot \frac{\sin(b \cdot t)}{b \cdot t} + f_i \cdot e^{-(t/T^*_{2,i})^{\upsilon_i}} + f_a \cdot e^{-(t/T^*_{2,a})^{\upsilon_a}} \quad (4)$$

where t is the acquisition time, $f_{c/i/a}$ is the amplitude of the corresponding decaying component, $T^*_{2,i/a}$ and $\upsilon_{a,\,i}$ are the shape parameters (apparent T_2 and stretching exponents υ) of the more mobile components, while *a*, *b* were the shape parameters of the crystalline part, where the so-called Abragamian function works well for polymers with only CH_2 groups along the main chain. **Figure 7** shows as an example an FID of PBS measured at 100 °C after isothermal crystallization for 48 h. For the assessment in the main paper, the crystalline contribution to the FID was isolated by subtract-

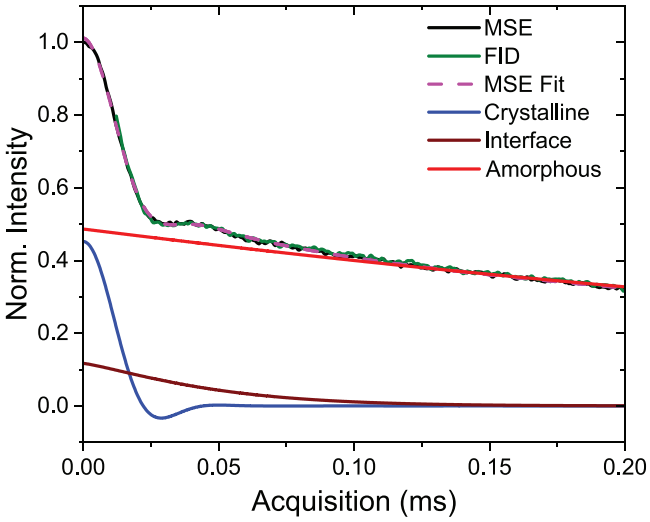

Figure 7. a) FID and MSE-FID of PBS (T_c = 100°C) as well as the three fitted components of the MSE-FID.

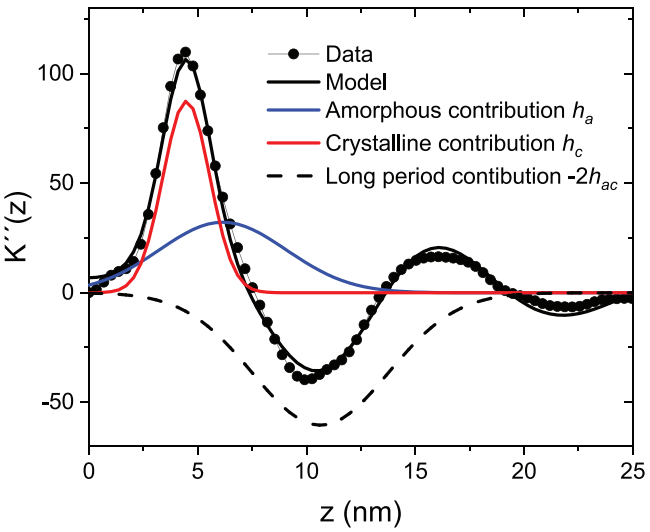

Figure 8. Exemplary result of SAXS analysis (T_c = 100°C, t_c = 49 h): Interface distribution function $K''(z)$ (IDF), as calculated from the scattering data and the corresponding model function together with the first three leading contributions, that is, crystalline contribution h_c, amorphous contribution h_a, and long period contribution $-2h_{ac}$. As the crystallinity measured by NMR was below 50%, h_c is assigned to the contribution with smaller mean value.

ing the fitted intermediate and amorphous fractions. The mass crystallinity was calculated according to

$$X_c = \frac{f_c}{f_c + f_i + f_a} \cdot 100\% \quad (5)$$

^{13}C MAS Spectroscopy:: All ^{13}C spectra and data were recorded on 400 MHz Bruker Avance III spectrometers with ^{13}C Larmor frequency of 100.6 MHz using double- and triple-resonance MAS probes at a spinning frequency of 10 000 ±3 Hz. The pulse lengths on the ^{1}H and ^{13}C channels were ≈3 µs. CP spectra were recorded with contact times of 0.1 ms for crystalline-signal selection as well as 1.5 ms for maximum signal overall, using an RD of 5-7 s (shorter at higher temperature) for near-complete T_1 relaxation of the ^{1}H nuclei (being the source of polarization in CP). In contrast, ^{13}C DP with short RD of ≈1 s emphasizes the mobile/amorphous signals. For measurements of the ^{13}C T_1 relaxation decay, the pulse sequence of Torchia[34] featuring a *z*-filter on the ^{13}C channel after CP was used, utilizing peak deconvolution to faithfully separate the different resonances.

SAXS:: SAXS measurements were performed on a Kratky compact camera (Anton Paar GmbH, Graz, Austria) equipped with an X-ray optics (AXO Dresden GmbH, Germany), a temperature-controlled sample holder, and a 1D detector Mythen2 R 1K (Dectris, Switzerland). As the camera has a slit focus, the data had to be deconvoluted. This was achieved by applying the desmearing algorithm by Strobl.[47]

The PBS samples were quenched from the melt state (150 °C) to different isothermal crystallization temperatures in the Kratky camera. The exposure time for each measurement was 10 min. The analysis of the SAXS data is based on the interface distribution function (IDF or K′′(z)), originally introduced by Ruland.[48] The detailed analysis procedure was described in previous publications.[13,15] Here, only a brief account of the method is given and one exemplary set of data is shown. The morphology of semicrystalline polymers was described as consisting of stacks of alternating crystalline and amorphous layers with sharp interfaces between the two regions. The IDF has the following form.

$$K''(z) = \frac{O_s \Delta\rho^2}{2}\left(h_a(z) + h_c(z) - 2h_{ac}(z) + h_{aca}(z) + \cdots\right) \quad (6)$$

where z is the coordinate perpendicular to the lamellar stacks, $\Delta\rho$ is the electron density difference between crystalline and amorphous regions, and O_s is the specific inner surface between crystalline and amorphous regions. Furthermore, $h_a(z)$ and $h_a(z)$ are the distributions of the amorphous and crystalline layer thicknesses. h_{ac} is the thickness distribution of the long period ($L = d_a + d_c$). We assume h_c and h_a to be normal distributions, higher order distributions are described as convolutions of the two fundamental distributions.[15]

$$h_{a,c}(z) = \frac{1}{\sqrt{2\pi}\sigma_{a,c}} e^{-\frac{(z-d_{a,c})^2}{2\sigma_{a,c}^2}} \quad (7)$$

Here $\sigma_{a,c}$ are the widths and $d_{a,c}$ are the mean values of the corresponding distributions. After background subtraction, the following relation holds between $K''(z)$ and the scattering intensity $I(s)$

$$K''(z) = 16\pi^3 \int_0^\infty [\lim_{s\to\infty} I(s)s^4 - I(s)s^4]\cos(2\pi sz)ds \quad (8)$$

where $s = \frac{2}{\lambda}\sin\theta$ is the scattering vector, $\lim_{s\to\infty} I(s)s^4$ is the Porod parameter P, which is determined under the constraint K″(0)=0. To suppress noise at high scattering vector, Equation (8) was multiplied by a window function $G(s) = e^{-4\pi^2 s^2 \sigma^2}$, where σ is the width of the window function. In this study σ = 0.6 nm was used. The cosine transform of the product of Equation (8) and the window function was fitted by the analytical model to determine the parameters d_c, d_a, σ_c, and σ_a.

Figure 8 shows and exemplary set of data obtained after a long isothermal crystallization of 49 h (2945 min) at T_c = 100 °C. Although the different contributions to the IDF overlap, they can be well separated with the quantitative modeling. The corresponding fit function in reciprocal space is shown in Figure S4, Supporting Information.

DSC:: DSC was performed with a DSC 8000 from Perkin Elmer. The sample was heated to 150 °C to remove thermal history and quenched to different crystallization temperatures. After the completion of isothermal crystallization, the sample was cooled to −60 °C and heated to 150 °C at a rate of 10 k min^{-1}.

Rheology:: The shear modulus was measured with a rheometer Ares G2 equipped with heating chamber from TA instruments using a sample

in stripe geometry (sample length between clamps 20 mm, width 10 mm, thickness 1.5 mm) at different temperatures but constant frequency of 10 rad s^{-1} and 0.1% strain. Beforehand the sample was isothermally crystallized at 100 °C in a rectangular mold (MeltPrep device) for 24 h, and then transferred to the rheometer at room temperature. The stepwise heating program for the measurement shown in Figure 6b was similar to that of the NMR-FID measurement.

Optical Microscopy:: Optical microscopy measurements were performed by using an Olympus BX51 microscope equipped with an Olympus XC30 camera allowing observation of the sample and recording of the images. A Linkam hotstage equipped with a Linkam TP 94 temperature controller and a Linkam LNP liquid nitrogen controller was used as the sample stage. 103 mg PBS was dissolved in 4 mL chloroform, and placed one droplet of the solution on a cover glass, which was heated to 140 °C to remove the solvent and melt the PBS. Another cover glass was placed on top of PBS melt. For the measurements, the sample (PBS sandwiched between cover glasses) was placed on the Linkam hot stage. The temperature was raised to 140 °C for 10 min and then cooled with a rate of 30 °C min^{-1} to different temperatures for isothermal crystallization. The crystallization was directly monitored using polarized light optical microscopy. Olympus Stream Motion software was used to observe the camera view on a computer and to analyze the images.

Supporting Information

Supporting Information is available from the Wiley Online Library or from the author.

Acknowledgements

The authors thank the Deutsche Forschungsgemeinschaft (DFG) for financial support in the framework of the SFB-TRR 102 (project-ID 189853844), project A1. Furthermore, the authors acknowledge K. Herfurt for technical help with DSC measurements and M. Schulz and M. Schaller for help in the early stages of the project.

Open access funding enabled and organized by Projekt DEAL.

Conflict of Interest

The authors declare no conflict of interest.

Data Availability Statement

The data that support the findings of this study are available from the corresponding author upon reasonable request.

Keywords

enthalpy of melting, intracrystalline chain diffusion, mechanical modulus, morphology, polybutylene succinate

Received: December 22, 2022
Revised: January 25, 2023
Published online:

[1] G. Strobl, *The Physics of Polymers. Concepts for Understanding their Structures and Behavior*, Springer, Berlin, Heidelberg **2007**.
[2] J. Hoffman, J. Lauritzen, *J. Res. Natl. Bur. Stand.* **1961**, *A 65*, 297.
[3] U. W. Gedde, *Polymer Physics*, 1st Edition, Chapman & Hall, London **1995**.
[4] D. Sadler, G. Gilmer, *Phys. Rev. Lett.* **1986**, *56*, 2708.
[5] D. M. Sadler, *Nature* **1987**, *326*, 174.
[6] S. Stepanow, *Phys. Rev. E* **2014**, *90*, 032601.
[7] E. Robelin-Souffache, J. Rault, *Macromolecules* **1989**, *22*, 3581.
[8] M. Hikosaka, *Polymer* **1987**, *28*, 1257.
[9] X. Jiang, G. Reiter, W. Hu, *J. Phys. Chem. B* **2016**, *120*, 566.
[10] A. Keller, M. Hikosaka, S. Rastogi, A. Toda, P. J. Barham, G. Goldbeck-Wood, *J. Mater. Sci.* **1994**, *29*, 2579.
[11] G. Strobl, *Eur. Phys. J. E* **2000**, *3*, 165.
[12] G. Strobl, *Rev. Mod. Phys.* **2009**, *81*, 1287.
[13] M. Schulz, A. Seidlitz, R. Kurz, R. Barenwald, A. Petzold, K. Saalwachter, T. Thurn-Albrecht, *Macromolecules* **2018**, *51*, 8377.
[14] M. Schulz, M. Schäfer, K. Saalwächter, T. Thurn-Albrecht, *Nat. Commun.* **2022**, *13*, 119.
[15] A. Seidlitz, T. Thurn-Albrecht, *Small-Angle X-Ray Scattering for Morphological Analysis of Semicrystalline Polymers*, Wiley, New York **2016**, pp. 151–164.
[16] M. Schulz, A. Seidlitz, A. Petzold, T. Thurn-Albrecht, *Polymer* **2020**, *196*, 122441.
[17] R. Muthuraj, M. Misra, A. K. Mohanty, *J. Appl. Polym. Sci.* **2018**, *135*, 45726.
[18] M. Peydayesh, M. Bagnani, R. Mezzenga, *ACS Sustainable Chem. Eng.* **2021**, *9*, 11916.
[19] O. Agboola, R. Sadiku, T. Mokrani, I. Amer, O. Imoru, *4 - Polyolefins and the Environment*, Woodhead Publishing, Sawston, Cambridge **2017**, pp. 89–133.
[20] W. Hu, K. Schmidt-Rohr, *Acta Polym.* **1999**, *50*, 271.
[21] Z. Zhai, C. Fusco, J. Morthomas, M. Perez, O. Lame, *ACS Nano* **2019**, *13*, 11310.
[22] Y. Otake, T. Kobayashi, H. Asabe, N. Murakami, K. Ono, *J. Appl. Polym. Sci.* **1995**, *56*, 1789.
[23] J. Xu, B. Heck, H. Ye, J. Jiang, Y. Tang, J. Liu, B. Guo, R. Reiter, D. Zhou, G. Reiter, *Macromolecules* **2016**, *49*, 2206.
[24] C. Schick, A. Toda, R. Androsch, *Macromolecules* **2021**, *54*, 3366.
[25] G. Z. Papageorgiou, D. N. Bikiaris, *Polymer* **2005**, *46*, 12081.
[26] M. L. Di Lorenzo, R. Androsch, *Crystallization of Poly[(R)-3-Hydroxybutyrate]*, Vol. *283*, Springer, Cham **2019**, pp. 119–142.
[27] C. Schick, R. Androsch, *Macromolecules* **2020**, *53*, 8751.
[28] S.-F. Yao, X.-T. Chen, H.-M. Ye, *J. Phys. Chem. B* **2017**, *121*, 9476.
[29] T. Miyata, T. Masuko, *Polymer* **1998**, *39*, 1399.
[30] K. Schäler, M. Roos, P. Micke, Y. Golitsyn, A. Seidlitz, T. Thurn-Albrecht, H. Schneider, G. Hempel, K. Saalwächter, *Solid State Nucl. Magn. Reson.* **2015**, *72*, 50.
[31] K. J. Ihn, E. S. Yoo, S. S. Im, *Macromolecules* **1995**, *28*, 2460.
[32] K. Schmidt-Rohr, H. Spiess, *Macromolecules* **1991**, *24*, 5288.
[33] Y. Yao, R. Graf, H. Spiess, D. Lippits, S. Rastogi, *Phys. Rev. E* **2007**, *76*, 060801.
[34] D. A. Torchia, *J. Magn. Reson.* **1978**, *30*, 613.
[35] K. Schäler, A. Achilles, R. Bärenwald, C. Hackel, K. Saalwächter, *Macromolecules* **2013**, *46*, 7818.
[36] M. Schäfer, S. Yuan, A. Petzold, R. A. Pérez-Camargo, A. J. Müller, T. Thurn-Albrecht, K. Saalwächter, K. Schmidt-Rohr, *Macromolecules* **2021**, *54*, 835.
[37] X. Wang, J. Zhou, L. Li, *Eur. Polym. J.* **2007**, *43*, 3163.
[38] M. Yasuniwa, S. Tsubakihara, T. Satou, K. Iura, *J. Polym. Sci., Part B: Polym. Phys.* **2005**, *43*, 2039.
[39] D. W. Van Krevelen, K. te Nijenhuis, *Properties of Polymers*, 4th Edition, Elsevier, Amsterdam **2009**.
[40] M. A. Kennedy, A. J. Peacock, L. Mandelkern, *Macromolecules* **1994**, *27*, 5297.
[41] Z. Bartczak, M. Kozanecki, *Polymer* **2005**, *46*, 8210.

[42] M. L. Di Lorenzo, R. Androsch, M. C. Righetti, *Eur. Polym. J.* **2017**, *94*, 384.
[43] T. Fujimaki, *Polym. Degrad. Stab.* **1998**, *59*, 209.
[44] W. Chen, D. Reichert, T. Miyoshi, *J. Phys. Chem. B* **2015**, *119*, 4552.
[45] W. Chen, W. Zhou, Y. Makita, S. Wang, S. Yuan, T. Konishi, T. Miyoshi, *Macromol. Chem. Phys.* **2018**, *219*, 1700451.
[46] R. Kurz, A. Achilles, W. Chen, M. Schäfer, A. Seidlitz, Y. Golitsyn, J. Kressler, W. Paul, G. Hempel, T. Miyoshi, T. Thurn-Albrecht, K. Saalwächter, *Macromolecules* **2017**, *50*, 3890.
[47] G. Strobl, *Acta Crystallogr., Sect. A: Cryst. Phys., Diffr., Theor. Gen. Crystallogr.* **1970**, *26*, 367.
[48] W. Ruland, *Colloid Polym. Sci.* **1977**, *255*, 417.